WARM NEUTRAL GAS AT REDSHIFT z=3.4

F. H. BRIGGS

Kapteyn Astronomical Institute, Postbus 800, 9700 AV Groningen, The Netherlands
Electronic mail: fbriggs@astro.rug.nl

E. BRINKS[1]

National Radio Astronomy Observatory, P.O. Box O, Socorro, New Mexico 87801-0387
Electronic mail: ebrinks@andromeda.cimat.mx

A. M. WOLFE

Center for Astrophysics and Space Science, C-011, University of California at San Diego, La Jolla, California 92093-0111
Electronic mail: art@cass150.ucsd.edu

ABSTRACT

Radio spectroscopy at 323 MHz using the Arecibo Telescope[2] and the VLA[3] has produced a tentative detection of the 21-cm line of neutral hydrogen at $z_{abs}=3.38716\pm0.00007$ in absorption against the radio continuum of the QSO MG 0201+113 ($z_{em}=3.61$). This redshift roughly agrees with one determined by the Westerbork Synthesis Radio Telescope and reported earlier; however the observations at different telescopes produce different results for width and optical depth of the line. If the detection holds, it provides evidence for a high column density of neutral gas that is confined to a dynamically cold layer with velocity dispersion ~10 km s^{-1}. Although the interpretation is uncertain due to a lack of detailed knowledge of the extended radio structure of the background quasar and the relative quantities of neutral gas in the cold and turbulent components, the observations specify high spin temperatures, $T_s \gtrsim 1000$ K for both this 21-cm line absorbing cloud and the turbulent component, which together have $N_{H\,I} \approx 10^{21.4}$ cm^{-2}. Results of optical spectroscopy require the additional presence of metal-enriched clouds of still broader velocity dispersion than the 21-cm line, creating a picture which is consistent with this system being a young disk galaxy that is sufficiently evolved by $z=3.4$ to have collapsed to a flattened system and produced a population of stars that have aged to pollute a turbulent halo. The observations constrain the neutral gas mass of a possible 21-cm line emitter associated with the intervening absorber to be less than $\sim(\Delta V/200\text{ km s}^{-1})10^{13}M_\odot$ for velocity widths ΔV (FWHM) in the range 200 to 1200 km s^{-1} ($H_0=100$ km s^{-1} Mpc^{-1}, $\Omega_0=1$). © 1997 American Astronomical Society. [S0004-6256(97)00402-0]

1. INTRODUCTION

The application of research into QSO absorption-lines to the field of galaxy formation relies on the interpretation that ordinary galaxies are likely to intervene at random along the line of sight to cosmologically distant background QSOs. This central hypothesis is verified by statistical tests for the "metal-line" and "damped Lyman α" systems, which are identified with galaxian halos and H I disks, respectively (cf. Sargent 1988; Wolfe 1988). At high redshift, where ordinary galaxies are too distant to be viewed in their own emitted light, QSO absorption-lines provide the only clues to the state of evolution for the bulk of the galaxy population. Clearly, objects with large gaseous cross sections and high space densities are the systems most frequently encountered. This paper shows that the MG 0201+113 $z_{abs}\approx3.4$ absorp-

tion system, which is a typical high redshift system selected on the basis of strong, damped Lyman α absorption (cf. Lanzetta 1993), has already collapsed to a low velocity dispersion layer. Analysis of the associated metal lines reveals an additional gaseous component of broader velocity spread that can be identified with a turbulent halo; in these respects, the findings are consistent with the 21-cm absorption systems discovered at lower redshifts (Briggs & Wolfe 1983; Wolfe 1986; Briggs 1988).

The Arecibo and VLA observations reported here for MG 0201+113 constrain the optical depth of the 21-cm absorption-line to be significantly less than the value reported by Baum *et al.* (1994) and de Bruyn *et al.* (1996) for this system, although the measured redshifts are in good agreement. Deduction of high spin temperature in the absorber are consistent with the findings of de Bruyn *et al.* (1996) and with determinations for other redshifted 21−cm absorption lines (Wolfe 1986; Briggs 1988; Cohen *et al.* 1994; Steidel *et al.* 1995; Carilli 1995; Carilli *et al.* 1996).

The new observations also place constraints on emission in the 21-cm line from a massive H I-rich structure, such as a "pancake" (Zel'dovich 1970) or collapsing galaxy proto-

---

[1]Currently on leave at Departamento de Astronomía, Universidad de Guanajuato, México.
[2]The National Astronomy and Ionosphere Center is operated by Cornell University under contract with the National Science Foundation.
[3]The National Radio Astronomy Observatory is a facility of the National Science Foundation operated under cooperative agreement by Associated Universities, Inc.

cluster, which might be associated with the damped Lyman α absorber (Wolfe 1993). Surveys to detect neutral hydrogen in emission at high redshift through the observation of the 21-cm line are now probing substantial volumes of space; Wieringa *et al.* (1992) present a review of recent surveys. Taramopoulos *et al.* (1994) conducted a recent VLA study of the environment of the $z \approx 3.4$ damped Lyman α absorber in the spectrum of Q0000−263 to perform a similar search for 21-cm emission.

2. THE ARECIBO OBSERVATIONS

Radio spectroscopy of a narrow band around the expected sky frequency of the redshifted 21-cm line for MG 0201 +113 was performed with the 318 MHz system of the Arecibo Telescope in sessions on 1993 October 7, 8, 18, 20, 26 and November 19, 23, 24, 25. The details of the instrumentation are given by Briggs *et al.* (1993). The only significant change since then has been the improvement of the RF preamplifier so that system temperatures as low as 65 K were measured on regions of sky far from the Galactic plane. A 2.5 MHz bandwidth signal from the single linear polarization available with the 318 MHz feed was fed to two parallel, 1024 channel banks of the Arecibo Correlator; the pair of resulting spectra were averaged to obtain a slight improvement in signal-to-noise ratio resulting from the different clip levels between the two banks, which were operated in the three-level mode. After a single Hanning smoothing, the spectra have a resolution of 4.88 kHz.

The observations were made in the "total-power mode," in which an on-source integration of 5 one-minute records was followed by a similar set of 5 records taken off-source at sky coordinates that are chosen to force the telescope to track through the same antenna coordinates as it did during the on-source scan. In order to calibrate the system gain as a function of frequency, similar ON-OFF scans were obtained for the bright radio source 0320+0523. The continuum spectrum of 0320+0523 is nearly flat for frequencies below 400 MHz so the flux density 7.63±0.18 Jy listed in the Texas Survey at 365 MHz (cf. Douglas *et al.* 1980) was adopted to fix the flux scale of the observation. Subtraction of each one-minute off-source spectrum from its corresponding on-source spectrum produced a set of difference spectra for both the calibration source and the program source, MG 0201 +113, and these difference spectra were carefully inspected to identify anomalous behavior. After excluding difference spectra that were corrupted by strong interference, the difference spectra for the calibration source were averaged to form gain functions for division into the difference spectra for the program sources to correct for the spectral dependence of the receiving system gain. A total of 270 one-minute difference spectra for MG 0201+113 remained after editing; 130 were discarded.

The "uncorrupted," gain-corrected, difference spectra for MG 0201+113 were averaged to form one spectrum for each of the 9 days on which observations were made. The weighted average of the 9 nine days is shown in Fig. 1(b) after continuum subtraction with a linear baseline. The standard error of the mean for each spectral point is shown in Fig. 1(a); it was computed from the scatter of the nine days

data about the mean. The standard error in the final spectrum was expected to be ∼2.8 mJy based on the sensitivity of the system and the net integration time. The variable nature of RFI signals causes afflicted channels to stand out in the plot of standard error, and this provides a basis for the automatic excision of corrupted channels from the plot in Fig. 1(c) whenever the standard error exceeds a threshold of 4.2 mJy, a value which was chosen by inspection to cut off the non-Gaussian tail of the distribution of standard errors. This removes the worst of the RFI but does not guarantee that all of it has been recognized. Regions have also been omitted at 323.01–323.03 and 323.30–323.33 MHz, where there is clear evidence for contamination in Figs. 1(a) and 1(b), even though they failed to be rejected automatically.

Both Figs. 1(b) and 1(c) show an absorption feature at a frequency consistent with the redshift determined from optical spectroscopy of the narrow metal absorption lines associated with the damped Lyman α line. Figure 2 displays a 0.5 MHz spectral band encompassing the absorption-line frequency along with Gaussian profiles that have been fitted to the feature. One of the fits relies on the linear baseline fitted to the entire edited spectrum and produces a line depth of 11.1±1.3 mJy. A linear baseline fit to the restricted spectral region shown in Fig. 2, with the exclusion of the absorption line itself, has a weak slope across the band and produces a slightly deeper line of 11.6±2.0 mJy. Both fits indicate a frequency centroid of 323.764±0.005 MHz and a width of 25±5 kHz (FWHM). These parameters correspond to a heliocentric redshift of 3.38716±0.00007 and a velocity width of $\Delta V = 23 \pm 5$ km s^{-1}. Considerable non-Gaussian noise remains in the spectra of Figs. 1 and 2, due to the low level RFI that is scattered throughout the band. Thus, systematic errors may add to the statistical uncertainties that are determined from the nonlinear least-squares fits to the absorption feature. The integrated on-source and off-source passband spectra were checked to be sure that the absorption feature did not arise from a slight excess of weak RFI in the off-source spectra. The results from the 9 days were also compared to ensure that the strength and Doppler corrected frequency of the feature is consistent with a celestial origin.

3. THE VLA OBSERVATIONS

The source MG 0201+113 was observed in D-array on 1989 November 10 and December 7 for 1 and 1.5 hour, respectively. The rms noise reached was only of order 20 mJy and was not expected to be sufficient to detect any absorption. The purpose of these observations was to test which observational setup was best suited for the project and to obtain a wide-field map over about 15 degrees. Note that the VLA, because of its antenna lay-out, collects visibilities in a three-dimensional volume rather than the usual two-dimensional uv-plane (see Perley 1989). This causes sources away from the field center to become increasingly distorted. This distortion is baseline dependent. Therefore, in order to be able to remove strong sources within the field of view from our high resolution observations, a low resolution map was essential to locate those sources.

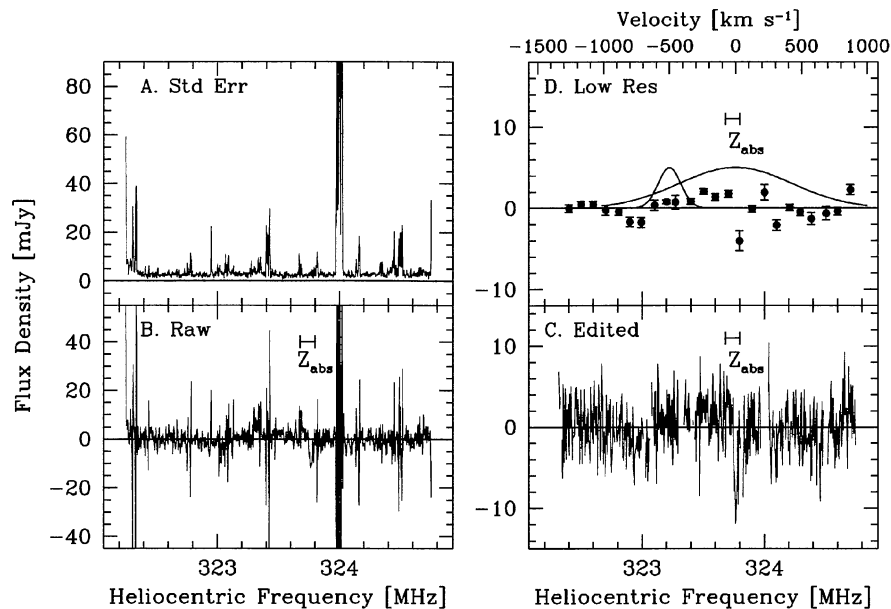The high resolution observations were made with the

FIG. 1. Spectrum of MG 0201+113. (a) *Top left panel.* Standard error in the raw spectrum as a function of frequency. (b) *Lower left panel.* The mean raw spectrum. The redshift for the optical lines (White *et al.* 1993) is marked by an error bar to indicate uncertainty in Z_{abs}. (c) *Lower right panel.* Edited spectrum after RFI excision. (d) *Top right panel.* Edited spectrum averaged to 100 kHz resolution. The Gaussian profiles represent $10^{13} M_{\odot}$ of H I with 200 km s^{-1} FWHM and $5 \times 10^{13} M_{\odot}$ of H I with 1000 km s^{-1} FWHM.

VLA in its B-configuration. We had six observing sessions, lasting 8 hours each, of which 6 hours were spent on target, on 1991 September 23 and October 24–28. We used 3C 48 as absolute flux calibrator, phase- and bandpass calibrator. The observations took place during reconfiguration from BnA to B-array, except for the September 23rd observations which were done while the array was mostly still in A-array. One of the antennae was located on one of the far stations on the eastern arm. Although it joined in the observations, it's disproportionally long baseline made it difficult to calibrate and we decided to remove this antenna from the data. Also for the 23rd September observations we had difficulties reaching the same level of accuracy as in the other five runs. In the end we decided not to use these data, resulting in a total of 30 useful hours on source.

The observations were made at a fixed frequency. Known VLA interference spikes were as far as possible centered in the middle of a channel to minimize ''ringing.'' The October data were obtained within one week at a time when MG 0201+113 transited at midnight and no correction for a change in Doppler shift due to the motion of the Earth around the Sun was necessary since the frequency offset was less than 2 kHz. In order to correct the September data to Heliocentric velocities, the data had to be shifted by 16.5 kHz.

The observations were done using a spectral line correlator mode in which the pre-amplified signal is sent through two different back-end filters. In this way we obtained two sets of data; we covered 0.781 MHz at a resolution after Hanning smoothing of 12 kHz using 64 channels. Simultaneously, we observed a 0.195 MHz range at 3 kHz resolution, again using 64 channels. We will concentrate in what follows on the lower resolution data.

Because of locally generated interference, which is most prominent at multiples of 12.5, 5, and 1 MHz, with lesser spikes at 100 kHz intervals, we had to discard the standard continuum channel, which is the average over the inner 75% of the band, and had to create a new continuum channel based on those channels which were free from interference and outside of the range where absorption was expected. From the viewpoint of an interferometer, interference appears to come from the direction of the North Pole. RFI affects synthesis maps with characteristic patterns corresponding to regions of the uv-plane where phase winding is low, i.e., along the v-axis. Therefore, a strip which was 0.05 kλ wide was discarded from the data.

After these steps, the data were edited and calibrated as usual within AIPS. Because the observations were done during reconfiguration, some antennas were either missing from the array, or had such uncertain baseline positions that we
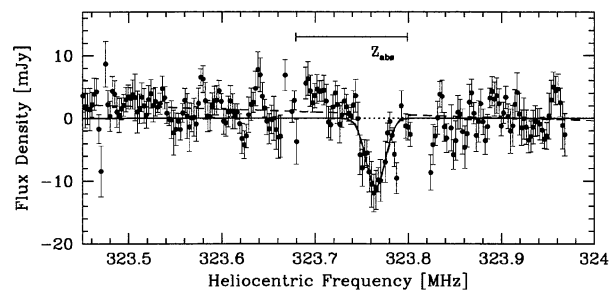

FIG. 2. Spectrum of MG 0201+113 showing the region of the 21-cm absorption line at 323.764 MHz. Error bars represent the standard error for each spectral point. The solid line shows the fit of a Gaussian line shape to the absorption line using the linear baseline fitted to the entire 2.5 MHz spectrum after RFI editing. A dashed line, rising to about +2 mJy at the left side of the plot a the baseline fitted to the limited portion of the spectrum shown in this plot excluding the region around the absorption line.

decided to delete them from the observations. On average, 22 antennae were present during each run. At 327 MHz the ionosphere introduces rapid phase variations. We used self-calibration (one phase self-calibration cycle, followed by one cycle correcting both phases and amplitudes) to improve upon the standard calibration. We used one main field and sixteen subfields within the task MX to incorporate as many of the brightest sources in the field as possible for the self-cal.

A critical step in the calibration is the bandpass correction. At 327 MHz, our target field contains some 15 J of flux density. In order for the final accuracy in the spectra to be determined by the thermal noise (or confusion limit) rather than by the rms in the determination of the bandpass correction, the bandpass calibrator needs to be exceedingly bright. The source 3C 48 is about 45 Jy, or $3\times$ the integrated flux in the field. By observing it for about one third of the time as the target field, we ensured that we were not limited by the spectral line dynamic range. Regarding the bandpass, we know that due to slight temperature variations within part of the waveguide system, the VLA bandpasses are time variable. A standing wave pattern with a roughly 3 MHz period moves as a function of time across the band (both in phase and amplitude). To minimize its impact on our observations, we observed 3C 48 every half an hour between observations on our target and applied the baseline solution which was closest in time to each target observation.

As was mentioned above, the D-array data were used to map a large, 15 degree, field around MG 0201+113. This map showed little distortion and some 40 sources with a total flux density (not corrected for beam attenuation) of about 10 Jy were located. Using the AIPS program MX we mapped small fields, accurately centered on each of these sources to obtain distortion free maps, and clean components, for all of them. Because of a limit to the number of fields MX can image at a time, half the sources, the strongest ones, were located first and subtracted from the uv-data using UVSUB. After this the second set of sources was dealt with.

The VLA observations measure the continuum flux density of MG 0201+113 to be 290±5 mJy at 330 MHz.

Note that it isn't possible to make a spectrum at the location of MG 0201+113 before any of the sources has been subtracted. The noise in the maps is dominated by sidelobes of the many sources in the field rather than thermal noise. At the time the data reduction was performed, there was no task which could perform distortion-free imaging of VLA B-array data and the number of fields which could be cleaned simultaneously was limited as well. After subtraction of the sources in the uv-plane as outlined above, we reached the expected thermal noise in an individual channel map of 6–7 mJy beam^{-1}. It should be noted, though, that still some non–Gaussian component to the noise is present. When averaging about 48 channels, the noise doesn't decrease below 3 mJy beam^{-1}. Luckily, the noise characteristics between individual days seem to be uncorrelated and averaging maps from the October run resulted in spectra with an average rms noise per channel of 2.8 mJy beam^{-1}.

Before creating these final spectra we clipped the visibility data at 6 sigma per individual baseline in order to remove random RFI spikes. Also, we removed the residual continuum emission from the final image cubes with the program IMLIN which fits a first order baseline (offset and slope) to the data.

These observations were performed in the same period as those by Uson *et al.* (1991a, 1991b) who identified a problem with the setting of the instrumental delays at 327 MHz, causing a subtle instrumental effect to contaminate their result (Uson, private communication). We checked our observations for a similar effect. However, our bandwidth was much narrower than theirs and any delay errors, visible as a slope in the phases of the bandpass calibrator, were small and were corrected to first order in the calibration process.

J. Uson, independently and using the program UVLIN to subtract continuum sources from the data cubes and remove interference spikes, re-reduced a few of our observations. He reached broadly similar noise levels, and the final spectra and maps were virtually identical.

The VLA spectrum is shown in Fig. 3(a). The error bars in this plot have been determined from the scatter of the measurements for the five days. The uncertainties computed in this way are expected to have a spread with standard deviation of $\sim 6.7/\sqrt{5} = 3.0$ mJy, although there are local variations. No significant absorption is seen in the VLA spectrum toward MG 0201+113 over the optical redshift range measured at a (local) 3σ level of 11 mJy beam^{-1}, although the upper panel of Fig. 3 shows there is a tendency for the broad-band data points in the vicinity of the Arecibo line to fall below the zero line and for points away from the center of the spectrum to lie above. The noise in the VLA spectra is higher than that obtained at Arecibo, and the two results are therefore in marginal agreement. However, neither the VLA nor Arecibo spectra are consistent with the Westerbork measurement of a line depth of 30 mJy, a width of 15 kHz, and a heliocentric frequency of 323.7766±0.002 MHz. The VLA measurement at this point is 6.1±6.2 mJy. Depending on which rms noise figure one prefers, the line depth measured at Westerbork would have corresponded at the VLA to a four to seven σ result.

We also extracted spectra towards some of the other strong sources in the field, since the Arecibo beam has a 16' beam that would include the spectra of a number of sources at the center of the VLA fields. No absorption was seen in any of the spectra over the frequency range covered. The channel maps for the five days were co-added and were inspected for low-level extended emission. Again, no emission at a level of 20 mJy over areas of typically 6 arcmin was seen.

Because the WSRT reported (de Bruyn *et al.* 1996) a line which was not resolved at 9 kHz resolution, we reduced the high frequency resolution data as well, using the same procedure as described above. As expected the high resolution spectra have a noise which is twice that of the low resolution data. The final spectrum is shown in Fig. 3(b). No feature was seen at the level reported by the WSRT, either in the high resolution spectra or in spectra smoothed to an intermediate resolution. When smoothing even further, to the level of the low resolution data, basically the same data, but processed through a different IF system, are recovered.
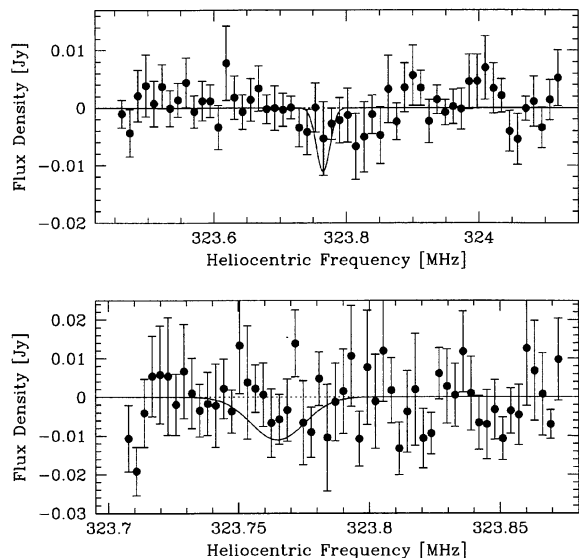
FIG. 3. VLA Spectra. The upper panel shows the low spectral resolution 12.2 kHz data. The lower panel shows the 3.05 kHz resolution spectrum. The Gaussian fit to the absorption-line measured in the Arecibo spectrum is drawn as a solid curve. Error bars were computed from the internal consistency of the spectra obtained from the 5 days of observation averaged to obtain the final spectra.

A comparison of the absorption line shapes measured by the three different telescopes is made in Table 1. The Arecibo and VLA measurements are consistent with each other but are inconsistent with the WSRT observation. An "integral line strength" of the sort computed in the following section for the purpose of estimating the gas spin temperature is also listed. These values are similar, since the WSRT line is both deeper and narrower by factors of approximately three than the Arecibo measurement; this explains why similar constraints are placed on spin temperature by de Bruyn *et al.* (1996) and us.

4. DISCUSSION

In principle, a comparison of the column density obtained from measurement of the Lyman α absorption-line with the optical depth measured in the radio can be used to specify the spin temperature of the absorbing gas, thus indicating the excitation level in this high redshift absorber. This line of reasoning has been pursued in a number of cases (Wolfe & Davis 1979; Wolfe *et al.* 1981; Wolfe *et al.* 1985). Here, we pursue this argument, pointing out the large uncertainties and leading to the conclusion that the result would be considerable strengthened by further radio studies to define the background quasar's radio continuum structure and new high-resolution optical spectroscopy to better define the complete kinematical model for this absorption system. Similar arguments have been made by de Bruyn *et al.* (1996) for this system.

Combination of the observed 21-cm line depth with the continuum strength produces a measure of optical depth at line center of $\tau_{21} = 0.037 \pm 0.008$. Adopting the column density determined from the strength of the damped Lyman α absorption line (White *et al.* 1993) $N_{\mathrm{H\,I}} = 10^{21.4}$ cm^{-1} and

TABLE 1. Comparison of line parameters at three telescopes.

Parameter	WSRT[a]	Arecibo[b]	VLA[c]
Optical Depth τ_{21} at line center	0.085 ± 0.02	0.037 ± 0.008	$< 0.05(23/\Delta V)^{1/2}$
Line Width (FWHM) ΔV km s^{-1}	9 ± 2	23 ± 5	—
Redshift, z_{abs} Heliocentric	3.38699 ± 0.00003	3.38716 ± 0.00007	—
$\int \tau_{21} dv$ km s^{-1}	0.77 ± 0.2	0.85 ± 0.2	$< 1.2(\Delta V/23)^{1/2}$

[a]Westerbork data from de Bruyn *et al.* (1996).
[b]Arecibo observations from this paper.
[c]The VLA observation reported in this paper places upper limits on the optical depth and integral line strength.

using the expression for the spin temperature, $\langle T_s \rangle = N_{\mathrm{H\,I}}/(1.823 \times 10^{18} \int \tau_{21}(v) dv)$ (cf. Dickey & Brinks 1988), yields an estimate for $\langle T_s \rangle \approx 1380$ K. This temperature is the column-density-weighted, harmonic mean of the spin temperature along the sight line (Kulkarni & Heiles 1987; Dickey & Lockman 1990). $\langle T_s \rangle \approx 1380$ K is substantially higher than is observed along lines of sight through the Milky Way Galaxy or M31 (Dickey & Brinks 1988), where $\langle T_s \rangle \sim 200$ to 300 K are typical for column densities $N_{\mathrm{H\,I}} \approx 10^{21}$ cm^{-2}. The estimate for T_s in the $z = 3.4$ absorber does have uncertainty in addition to those attached to τ_{21} and ΔV; we estimate the uncertainty in $N_{\mathrm{H\,I}}$ to be $\sim 30\%$, which is not enough to alter the conclusion that $\langle T_s \rangle$ computed in this way is high.

We have assumed that all the neutral gas that contributes to the damped Lyman α profile is confined to the Gaussian feature that we observed in the 21-cm line. A sharply contrasting possibility is that the high redshift system has substantial quantities of warm, low optical depth gas that is sufficiently spread in velocity to escape inclusion in the 21-cm profile. Then, the inferred T_s for the 21-cm absorber becomes $\simeq T_s f_{21}$, where f_{21} is the fraction of $N_{\mathrm{H\,I}}$ that is contained in the 23 km s^{-1} profile (velocity dispersion $\sigma \approx 10$ km s^{-1}). Thus, in addition to the narrow 21-cm absorption component, a complete description of the kinematics of the system must include the broader, low column density component whose cloudlets are optically thick in the resonance lines of common metals but optically thin in the 21-cm line. In other systems at lower z, this component has been tentatively identified with halo gas that encases the dynamically cold, 21-cm absorbing disk (Wolfe & Wills 1977; Briggs & Wolfe 1983; Briggs *et al.* 1985; Lanzetta & Bowen 1992). For these cases, high-resolution optical spectroscopy has led to the general conclusion that most of the neutral column density in the damped Lyman α systems is concentrated in the cold, low-dispersion component (cf. Wolfe *et al.* 1994), and only a tiny fraction of the neutral gas is contained in the broad, turbulent (or "halo") component, which dominates in providing the equivalent widths measured for the metal lines. Thus, f_{21} is likely to be close to unity, and $T_s \approx 1380$ K as indicated above.

For this system in absorption against MG 0201+113, the effective velocity spread of the broad component can be es-
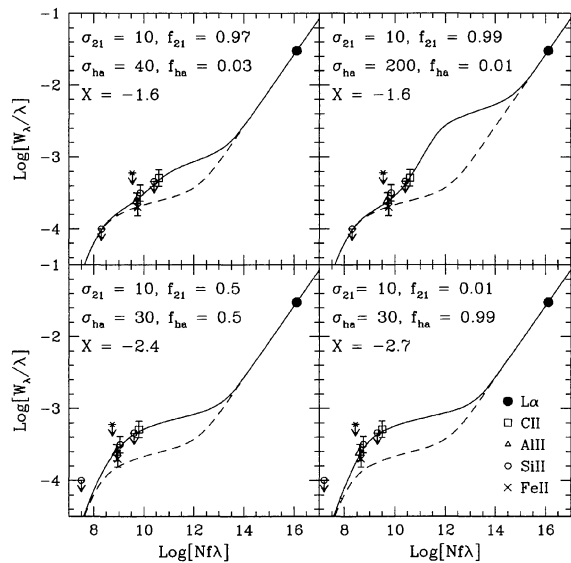
FIG. 4. Curve of Growth (COG) display of the range of two-component kinematical models that simultaneously fit both the 21-cm line profile and the ultraviolet lines. The *top panels* illustrate the range of models with the highest metal abundances (relative to solar abundances) and lowest fraction of neutral gas in the broad velocity dispersion, "halo" component. The *lower panels* explore the range of models with the large fractions of gas in the "halo" component, yielding the lowest values of metal abundances. The dashed COG represents the $\sigma_{21} = 10$ km s^{-1} 21-cm absorption component. The solid line is the two component model. The damping portion of the COG is drawn for Lyman α. The abscissa has units of cm^{-1}.

FIG. 5. Constraints on spin temperature as a function of the fraction of the neutral gas contained in the 21-cm component, f_{21}. The fraction of gas contained in the broad velocity dispersion "halo" component, $f_{\text{halo}} = 1 - f_{21}$, is plotted across the top horizontal axis. *Upper panels* indicate the range of effective velocity dispersions, σ, and lower limit to spin temperature, T_{spin}, for the "halo" component, determined from the COG analysis of Fig. 4 and the detection limits in the 21-cm line. The *lower-central panel* plots the logarithm of the metal abundance relative to solar, assuming that it is the same in both components. The *lower panel* plots the spin temperature of the 21-cm line component as a function of f_{21}.

timated from the equivalent widths of the metal lines observed in the low resolution (10 Å) spectra of White *et al.* (1993). We performed a curve of growth analysis using the line depths and limits to depth for several transitions of Si II ($\lambda 1260$, $\lambda 1526$, $\lambda 1808$), Fe II ($\lambda 1144$, $\lambda 1608$), C II ($\lambda 1334$), and Al II ($\lambda 1670$). Although there is considerable uncertainty in this analysis, it serves to illustrate the constraints on the parameters that need to be specified to better determine the spin temperature. A range of two component models is illustrated in Fig. 4: the cold cloud has $\sigma_{21} = 10$ km s^{-1} and $N_{21} = f_{21} N_{\text{H I}}$, and the "halo" component is modeled as a single broad dispersion cloud with σ_{ha} and neutral hydrogen column density $N_{\text{ha}} = f_{\text{ha}} N_{\text{H I}} = (1 - f_{21}) N_{\text{H I}}$. Due to the scarcity of information, a single measure for the metal abundances relative to solar abundances "X" is assumed for all ions in both components; for example, the total column density of C II in the system is specified by $N_{\text{C II}} = 10^X N_{\text{H I}} \times [n_C / n_H]_\odot$, where $[n_C / n_H]_\odot$ is the solar abundance of carbon relative to hydrogen as tabulated by Spitzer (1978). This approach also assumes that the carbon associated with the $N_{\text{H I}}$ in this layer is predominantly singly-ionized, in keeping with neutral clouds along lines of sight through the Milky Way Galaxy. The upper panels of Fig. 4 illustrate models in which the 21-cm absorber dominates the neutral column density; the lack of detection of the Si II $\lambda 1808$ line enforces a low metal-abundance estimate, and the stronger detections of other metal lines indicates that there is additional, turbulent gas. The data permit the velocity spread of the turbulent component to be very broad, although the C II line would be resolved by the instrumental resolution if
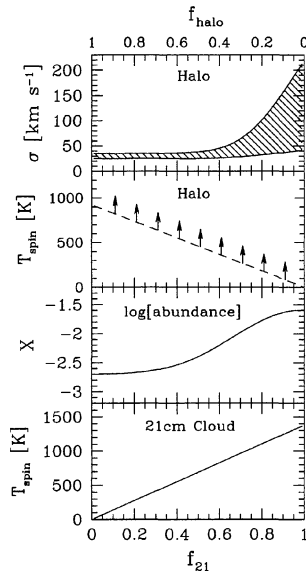
the effective σ were much over 200 km s^{-1}. The low resolution spectroscopy is compatible with a wide range of models. For example, the metal line strengths are also compatible with much larger fractions of gas lying in the broad component, as is shown in the lower panels of Fig. 4; this range of models must have much lower metal abundances.

The constraints on the relative column densities in the turbulent and cold components can be translated into measurements of the spin temperatures for both. These spin temperatures and the other model parameters from the COG analysis are summarized in Fig. 5. The metal abundances from the models range from $10^{-1.6}$ to $10^{-2.7}$ below solar. The lower limit to the spin temperature of the turbulent halo component results from inspecting the spectra in Figs. 2 and 3 and noting that an absorption-line three times broader than the detected line would probably escape detection if its depth were less than ~ 5 mJy. Although f_{21} is expected to be close to unity, the certainty of the interpretation would benefit from new, high-resolution optical spectroscopy that can demonstrate that the bulk of the gas is confined to the 21-cm line velocity width.

Further uncertainty in determination of the spin temperature results from possible differences in the spatial extent of the absorber and the background radio source, which may be substantially larger than the source of optical continuum causing a significant portion of the radio flux to leak around the thick absorbing cloud that creates the damped Lyman α line. The continuum map at 18 cm wavelength (Stanghellini *et al.* 1990) hints that this might be the case by showing evidence for a weak component extending to $\sim 4''$ from the

nucleus, although the extended emission accounts for only a tiny fraction of the total radio flux. While MG 0201+113 falls in the GHz–Peaked-Spectrum class of radio source, the integral flux density spectrum for the source shows a flattening at meter wavelengths (O'Dea *et al.* 1990), indicating that at the frequency of the redshifted 21-cm absorption line, the source is dominated by a more extended component than the compact optically thick core component that gives rise to the GHz peak in the continuum spectrum (de Bruyn *et al.* 1996). High resolution 90 cm VLBI observations are capable of defining the continuum source structure, which ultimately will clarify the interpretation. If the resulting $\langle T_s \rangle$ remains high, then the neutral medium in this absorber is substantially hotter than the neutral ISM of the Milky Way or M31. This may indicate that a larger fraction of the total H I is in the Warm Neutral phase with $T \approx 8000$ K (Kulkarni & Heiles 1987), or alternatively, the gas in the Cold phase that we detect in the 21-cm line may actually be hotter due to the inability of the gas to cool itself when the metal abundances are low.

The new Arecibo H I spectroscopy also places limits on the emission from large, neutral gas masses that might be associated with the damped Lyman α site. The sensitivity is a strong function of the velocity width of the signal (cf. Wieringa *et al.* 1992), which would be expected to range from a few hundred km s^{-1} for pancakes (Zel'dovich 1970) to more than 1000 km s^{-1} for analogs to present day galaxy clusters. Two examples of Gaussian profiles for $\Delta V = 200$ km s^{-1}, $M_{\mathrm{H\,I}} = 10^{13} M_\odot$ and $\Delta V = 1000$ km s^{-1}, $M_{\mathrm{H\,I}} = 5 \times 10^{13} M_\odot$ ($H_0 = 100$ km s^{-1} Mpc^{-1} and $\Omega_0 = 1$) are plotted in Fig. 1(d) for comparison with the data of Fig. 1(c), after averaging to 100 kHz wide spectral bins. Only a single linear baseline has been subtracted from the entire 2.5 MHz band. The choice of the narrow 2.5 MHz band for this experiment limits would prevent the detection of $\Delta V \gtrsim 1200$ km s^{-1}. Clearly, systematic effects, such as a weak, characteristic "standing wave" and low level RFI, dominate in limiting the sensitivity to broad signals. On the other hand, signals as large as these would be noticeable. The limits are still more than a factor of 10 higher than Wolfe's (1993) prediction for the amount of H I associated with damped Lyman α sites.

REFERENCES

Baum, S. A., de Bruyn, A. G., & O'Dea, C. P. 1994, BAAS, 25, 1401
Briggs, F. H., & Wolfe, A. M. 1983, ApJ, 268, 76
Briggs, F. H., Turnshek, D. A., Schaeffer, J., & Wolfe, A. M. 1985, ApJ, 293, 387
Briggs, F. H., Sorar, E., & Taramopoulos, A. 1993, ApJ, 415, L99
Briggs, F. H. 1988, in QSO Absorption Lines: Probing the Universe, edited by J. C. Blades, D. A. Turnshek, and C. A. Norman (Cambridge University Press, Cambridge), p. 275
Carilli, C. L., Lane, W., de Bruyn, A. G., Braun, R., & Miley, G. K. 1996, AJ, 111, 1830
Carilli, C. L. 1995, JA&A, 16, 163
Cohen, R. D., Barlow, T. A., Beaver, E. A., Junakharinen, V. T., Lyons, R. W., & Smith, H. E. 1994, ApJ, 421, 453
de Bruyn, A. G., O'Dea, C. P., & Baum, S. A. 1996, A&A, 305, 450
Dickey, J. M., & Brinks, E. 1988, MNRAS, 233, 781
Dickey, J. M., & Lockman, F. J. 1990, ARA&A, 28, 215
Douglas, J. N., Bash, F. N., Torrence, G. W., & Wolfe, C. 1980, The Texas Survey, Preliminary +18° Strip (University of Texas Radio Astronomy Observatory and Department of Astronomy, Austin)
Kulkarni, S.R., & Heiles, C. 1987, in Interstellar Processes, edited by D. J. Hollenbach and H. A. Thronson (Reidel, Dordrecht), p. 87
Lanzetta, K. M., & Bowen, D. V. 1992, ApJ, 391, 48
Lanzetta, K. L. 1993, in The Environment and Evolution of Galaxies, edited by J. M. Shull and H. A. Thronson (Kluwer, The Netherlands), p. 237
O'Dea, C. P., Baum, S. A., Strenghellini, C., Morris, G. B., Patnaik, A. R., & Gopal-Krishna, 1990, A&AS, 84, 549
Perley, R.A. 1989, in Synthesis Imaging in Radio Astronomy, ASP Conf. Ser. 6, edited by R. A. Perley, F. R. Schwab, and A. H. Bridle (Brigham Young University Print Services, Provo, Utah), p. 259

Sargent, W. L. W. 1988, in QSO Absorption Lines: Probing the Universe, edited by J. C. Blades, D. A. Turnshek, and C. A. Norman, (Cambridge University Press, Cambridge), p. 1
Spitzer, L. 1978, Physical Processes in the Interstellar Medium (Wiley, New York), p. 4
Stanghellini, C., Baum, S. A., O'Dea, C. P., & Morris, G. B. 1990, A&A, 233, 379
Steidel, C. C., Bowen, D. V., Blades, J. C., & Dickenson, M. 1995, ApJ, 440, L45
Taramopoulos, A., Briggs, F. H., & Turnshek, D. A. 1994, AJ, 107, 1937
Uson, J. M., Bagri, D. A., & Cornwell, T. J. 1991a, Phys. Rev. Lett., 67, 3328
Uson, J. M., Bagri, D. A., & Cornwell, T. J. 1991b, ApJ, 377, L65
Wieringa, M. H., de Bruyn, A. G., & Katgert, P. 1992, A&A, 256, 331
White, R. L., Kinney, A. L., & Becker, R. H. 1993, ApJ, 407, 456
Wolfe, A. M., & Wills, B. J. 1977, ApJ, 218, 39
Wolfe, A. M., & Davis, M. M. 1979, AJ, 84, 699
Wolfe, A. M., Briggs, F. H., & Jauncey, D. L. 1981, ApJ, 248, 460
Wolfe, A. M., Briggs, F. H., Turnshek, D. A., Davis, M. M., & Smith, H. E. 1985, ApJ, 294, L67
Wolfe, A. M. 1986, PTRSL, 320, 433
Wolfe, A. M. 1988, in QSO Absorption Lines: Probing the Universe, edited by J. C. Blades, D. A. Turnshek, and C. A. Norman (Cambridge University Press, Cambridge), p. 297
Wolfe, A. M. 1993, ApJ, 402, 411
Wolfe, A. M., Fan, X., Tytler, D., Vogt, S. S., Keane, M. J., & Lanzetta, K. M. 1994, ApJ, 435, L101
Zel'dovich, Ya. B. 1970, A&A, 5, 84